Modeling carrier transport in mid-infrared VCSELs with type-II superlattices and tunnel junctions

Modeling carrier transport in mid-infrared VCSELs with type-II superlattices and tunnel junctions

Valerio Torrelli*, Jesus Alberto Gonzalez Montoya*, Alberto Tibaldi*†, Pierluigi Debernardi†,
Andrea Simaz‡, Mikhail A. Belkin‡, Michele Goano*†, and Francesco Bertazzi*†
* Dipartimento di Elettronica e Telecomunicazioni, Politecnico di Torino, Corso Duca degli Abruzzi 24, 10129 Torino, Italy
† CNR-IEIIT, Corso Duca degli Abruzzi 24, 10129 Torino, Italy
‡ Walter Schottky Institute c/o Technical University of Munich, Garching, Germany
E-mail: alberto.tibaldi@polito.it

***Abstract*—Vertical-cavity surface-emitting lasers are promising light sources for sensing and spectroscopy applications in the mid-infrared $3 \div 4\,\mu$m spectral region. A type-II superlattice active region is used for carrier injection and confinement, while a buried tunnel junction defines a current aperture, decreasing the series resistivity. Highly nanostructured to optimize device performance, mid-infrared VCSELs pose modeling challenges beyond semiclassical approaches. We propose a quantum-corrected semiclassical approach to device design and optimization, complementing a drift-diffusion solver with a nonequilibrium Green's function description of band-to-band tunneling in the buried tunnel junction, and a local density of states computed from the solution of the Schrödinger equation in the superlattice active region.**

I. Introduction

Vertical-cavity surface-emitting lasers (VCSELs) are of significant interest for gas detection in the spectral region around $3 \div 4\,\mu$m, where many hazardous gases present strong absorption lines [1]. The 6.1 Å semiconductor family, including GaSb, AlSb, InAs and their related compounds, seems a promising material system to realize electrically pumped VCSELs emitting at a wavelength longer than $3\,\mu$m [2]. The antimonides are already emerging in the field of infrared imaging technology [3], due to their unique tunability capabilities of the detection wavelength over most of the technologically-relevant infrared spectrum, and the possibility of realizing different energy-band alignments, from type-I to type-II broken-gap (misaligned, or type III) superlattices [4]. Inspired by the nonequilibrium Green's function (NEGF) modeling of type-II superlattice photodetectors [5] and of near-infrared tunnel-junctions VCSELs, we present a quantum-corrected semiclassical drift-diffusion model to advance the understanding of the physics of carrier transport in mid-infrared VCSELs.

We consider the VCSEL described in [2]. The structure, emitting at $4\,\mu$m, is grown on a GaSb substrate; the resonant cavity is embedded between a bottom semiconducting distributed Bragg reflector (DBR) consisting of GaSb/$AlAs_{0.08}Sb_{0.92}$ and a top dielectric DBR based on ZnS/Ge alternating layers. To minimize absorption losses, electrical pumping is performed only within the cavity, leaving out the DBRs, by means of intracavity contacts. The radial current confinement is achieved with a buried tunnel junction (BTJ), reducing the p-doped portion of the device with respect to the *pin* design, and increasing the conductivity [6]. The portion of the device embedded within the contacts includes: two n-type GaSb spreading layers; an n-type InAs/AlSb chirped superlattice (SL), injecting electrons in the quantum wells (QWs) while simultaneously blocking backward hole propagation; the intrinsic active region includes a type-II superlattice with eight elements (each of them consisting of a 3.2 nm-thick $Ga_{0.9}In_{0.1}Sb$ hole-confining layer, placed between two 2.1 nm-thick InAs electron-confining layers, and one 3 nm-thick $Al_{0.35}Ga_{0.65}Sb$ barrier); a p-type $Al_{0.37}Ga_{0.63}Sb$ electron-blocking layer (EBL), also used for hole injection, and finally a 38 nm-thick heavily doped (2×10^{19} cm^{-3}) p^+-GaSb/n^+-$InAs_{0.91}Sb_{0.09}$ BTJ.

II. Numerical simulation and results

Lacking any description of quantum confinement and tunneling, a conventional drift-diffusion (DD) model would not be applicable to the analysis of the VCSEL structure under study. On the other hand, given the large extension of the device (thicker than $3\,\mu$m), the use of a genuine-quantum technique, such as the nonequilibrium Green's functions (NEGF) formalism [3], [5], [7], would not be feasible, due to its staggering computational cost. A numerical technique able to overcome these issues is obtained by extending the DD approach presented in [8]–[10] with an appropriate description of quantum effects in the BTJ and in the superlattice active region.

Different tunneling models have been proposed to describe carrier transport in a BTJ within the DD framework [11]–[13], but the lack of predictive capabilities limits their application to the case under study. Here, we follow the procedure described in [6], [14] in the context of near-infrared VCSELs for short-range optical communications. A multiband NEGF analysis of the BTJ is carried out to extract the tunneling current, from which a local band-to-band tunneling (BTBT) generation rate can be defined. The BTBT rate is included as a generation term in the continuity equations, in addition to the usual generation/recombination mechanisms (Auger, Shockley-Read-Hall and radiative).

Following the Poisson-Schrödinger-drift-diffusion (PSDD) approach developed in [5], we correct the local density of

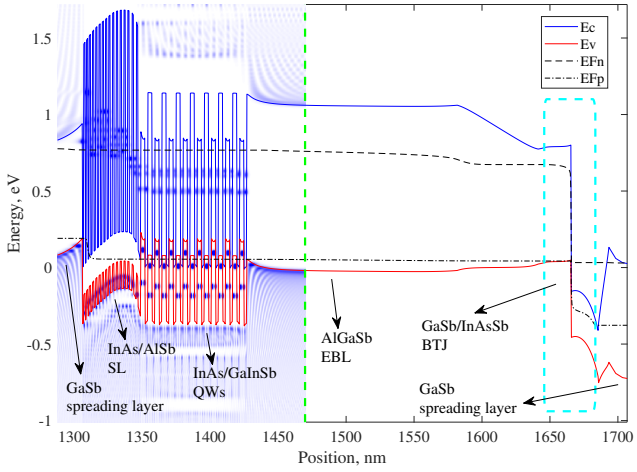

Fig. 1. Band diagram of the VCSEL under study biased at 0.8 V. Shades of blue represent the LDOS computed for normal incidence (zero transverse wavevector). Clearly visible is the formation of minibands in the superlattice active region. The green dashed line marks the end of the quantum-corrected region, beyond which the LDOS approaches the expected bulk behaviour. The region marked by the cyan box represents the BTJ region, where the NEGF simulation is carrier out to compute the BTBT generation rate. Most of the material parameters were taken from [15].

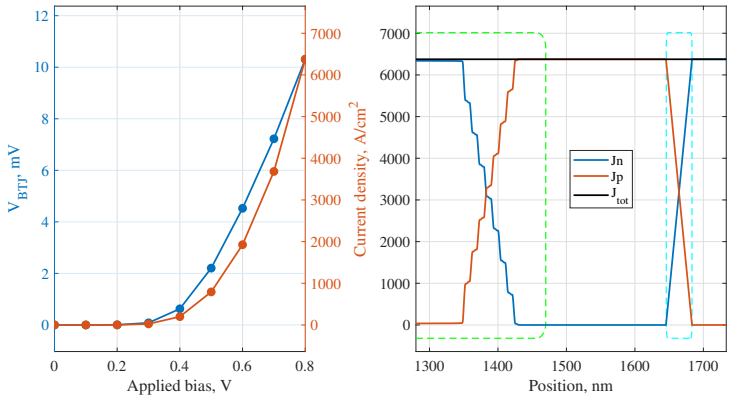

Fig. 2. Voltage drop over the BTJ and overall current density as a function of the applied voltage (left) and decomposition of the overall current density in terms of electron and hole current densities as a function of the position at a bias of 0.8 V (right). The green and the cyan boxes represent the quantum-corrected region and the BTJ region, respectively.

states (LDOS) in the active region by solving the Schrödinger equation in a multiband k·p basis [3]. The resulting charge, computed according to the quasi-Fermi levels provided by the DD solver, accounts for quantization and tunneling effects, raising and lowering the "effective" conduction/valence band edges seen by the carriers. For computational efficiency, the solution of the Schrödinger equation is restricted to the region where the quantum potential is nonzero, see color maps in Fig. 1.

Since in [2] continuous-wave operation was demonstrated down to $-40\,^{\circ}\mathrm{C}$, we performed the simulations at the same temperature, with an applied bias voltage ranging from 0 to 0.8 V. The band diagram and the LDOS computed for normal incidence are reported in Fig. 1. The chirped superlattice is designed to allow efficient injection of electrons via tunneling from the left spreading layer and subsequent electron relaxation to the conduction miniband in the active region, while simultaneously blocking of holes diffusing from the opposite side.

Fig. 2 (left) shows the fraction of the bias voltage that drops across the BTJ (V_{BTJ}) and the IV characteristics. V_{BTJ} is smaller than 10 mV at a bias voltage of 0.8 V, resulting in a current density of 6.38 kA/cm^2, which, when multiplied by the BTJ area (with a diameter of 12 μm), gives the indicative value of 7.2 mA. This estimate is compatible with the IV characteristics reported in [2] and confirms the high conductivity of narrow-gap type-III BTJs [16].

Fig. 2 (right) shows the decomposition of the total current density in terms of electron and hole contributions. The BTJ converts the electron current injected by the top contact into a current of holes, which diffuse towards the superlattice active region where they recombine radiatively. Due to the stronger localization of holes, the radiative transitions mostly occur in the $Ga_{0.9}In_{0.1}Sb$ QWs, giving rise to a well-defined staircase behaviour in the electron and hole currents. The similar steps in the staircase are indicative of an almost homogeneous occupancy of the eight QWs, again confirming the expectations in [2].

References

[1] L. S. Rothman, *et al.*, *J. Quant. Spectrosc. Radiat. Transf.* **110**, 533 (2009).
[2] G. K. Veerabathran, S. Sprengel, A. Andrejew, M.-C. Amann, *Appl. Phys. Lett.* **110**, 071104 (2017).
[3] F. Bertazzi, A. Tibaldi, M. Goano, J. A. Gonzalez Montoya, E. Bellotti, *Phys. Rev. Appl.* **14**, 014083 (2020).
[4] A. Rogalski, P. Martyniuk, M. Kopytko, *Appl. Phys. Rev.* **4**, 031304 (2017).
[5] A. Tibaldi, *et al.*, *Phys. Rev. Appl.* **16**, 044024 (2021).
[6] A. Tibaldi, *et al.*, *Phys. Rev. Appl.* **14**, 024037 (2020).
[7] U. Aeberhard, *Phys. Rev. B* **87**, 081302(R) (2013).
[8] A. Tibaldi, F. Bertazzi, M. Goano, R. Michalzik, P. Debernardi, *IEEE J. Select. Topics Quantum Electron.* **25**, 1500212 (2019).
[9] P. Debernardi, *et al.*, *IEEE J. Select. Topics Quantum Electron.* **25**, 1700914 (2019).
[10] A. Gullino, A. Tibaldi, F. Bertazzi, M. Goano, P. Debernardi, *MDPI Appl. Sci.* **11**, 6908 (2021).
[11] A. Schenk, *Solid-State Electron.* **36**, 19 (1993).
[12] J.-Y. Duboz, B. Vinter, *J. Appl. Phys.* **126**, 174501 (2019).
[13] A. Pan, C. O. Chui, *J. Appl. Phys.* **116**, 054508 (2014).
[14] A. Gullino, *et al.*, *21st International Conference on Numerical Simulation of Optoelectronic Devices (NUSOD 2021)* (online, 2021), pp. 79–80.
[15] I. Vurgaftman, J. R. Meyer, L. R. Ram-Mohan, *J. Appl. Phys.* **89**, 5815 (2001).
[16] K. Vizbaras, M. Törpe, S. Arafin, M.-C. Amann, *Semiconductor Sci. Technol.* **26**, 075021 (2011).